HRTEM observations of La2Zr2O7 thin layers on LaAlO3 obtained by chemical methods

L. Rapenne, Carmen Jiménez, Tristan Caroff, C. Millon, Stéphanie Morlens, Pascale Bayle-Guillemaud, François Weiss

High-resolution transmission electron microscopy observations of $La_2Zr_2O_7$ thin layers on $LaAlO_3$ obtained by chemical methods

L. Rapenne and C. Jiménez[a)]
Laboratoire des Matériaux et du Génie Physique (LMGP)—UMR 5628 Centre National de la Recherche Scientifique (CNRS)—Grenoble INP, Grenoble 38016, France

T. Caroff and C. Millon
Laboratoire des Matériaux et du Génie Physique (LMGP)—UMR 5628 CNRS—Grenoble INP, Grenoble 38016, France; and Consortium de Recherche pour l'Emergence de Technologies Avancées (CRETA)—Centre National de la Recherche Scientifique (CNRS) UPS2070, Grenoble 38042, France

S. Morlens
Consortium de Recherche pour l'Emergence de Technologies Avancées (CRETA)—Centre National de la Recherche Scientifique (CNRS) UPS2070, Grenoble 38042, France

P. Bayle-Guillemaud
CEA-Grenoble, INAC/SP2M/LEMMA, Grenoble 38054 Cedex 9, France

F. Weiss
Laboratoire des Matériaux et du Génie Physique (LMGP)—UMR 5628 Centre National de la Recherche Scientifique (CNRS)—Grenoble INP, Grenoble 38016, France

(Received 30 June 2008; accepted 11 December 2008)

$La_2Zr_2O_7$ (LZO) films have been grown by metalorganic decomposition (MOD) to be used as buffer layers for coated conductors. LZO can crystallize into two similar structures: fluorite or pyrochlore. Coated conductor application focuses on pyrochlore structure because it is a good barrier against oxygen diffusion. Classical x-ray diffraction is not able to separate the contribution of these two structures. Transmission electron microscopy and high-resolution transmission electron microscopy were used to determine the local distribution of these two phases in epitaxial LZO layers grown on $LaAlO_3$. A characteristic feature of LZO thin films deposited by MOD is the formation of nanovoids in an almost single-crystal structure of LZO pyrochlore phase. For comparison, LZO layers deposited by metalorganic chemical vapor deposition were also studied. In this last case, the film is compact without voids and the structure corresponds to pyrochlore phase. Thus, the formation of nanovoids is a characteristic feature of MOD grown films.

I. INTRODUCTION

Coated conductors developed from rolling-assisted biaxially textured substrates (RABiTs) are considered a low-cost architecture: nickel-based textured substrate is used as a template to biaxially grow the superconducting $YBa_2Cu_3O_7$ (YBCO) layer.[1] Nevertheless, the YBCO layer cannot be deposited directly on nickel because of the chemical interaction of nickel with YBCO at the usual deposition temperature. Buffer layers filling several characteristics (for instance, structural and chemical compatibility between substrate and active layer) have to be used between the substrate and the superconducting layer. Good results are obtained when using lanthanum zirconate, $La_2Zr_2O_7$ (LZO), as the first buffer layer. Metal organic decomposition (MOD) allows the growth of LZO on Ni-based substrates in reducing atmosphere, which avoids the undesirable oxidation of the substrate. This material has already been probed on a simple low-cost architecture obtained by all-chemical routes $YBCO_{MOCVD}/LZO_{MOD}/NiW_{RABiTS}$ in a previous work.[2]

Pyrochlore LZO behaves as a buffer layer in this architecture because its lattice parameters match those of YBCO [$|(\varepsilon_{YBCO}-\varepsilon_{LZO})/\varepsilon_{LZO}| = 1.05\%$], and also because it provides a good barrier against O_2 diffusion.[3] LZO pyrochlore structure (Space Group: $Fd\bar{3}m$, 73-0444, lattice parameter a = 10.808 Å) is derived from the LZO fluorite structure (Space Group: $Fm\bar{3}m$, 75-0346, lattice parameter a = 5.407 Å) with one-eighth of the anions absent and two distinct cation sites. Ni-based RABiTs present a cubic texture $\{100\}\langle 001\rangle$ (Space Group: $Fm3m$, 05-0850, lattice parameter a = 3.5238 Å); so it is well adapted to ensure the epitaxial growth of the LZO layer with the unit cell rotated to 45° to match the LZO unit layer: the epitaxial relationships are $[100]_{Ni}//[110]_{LZO}$ $[010]_{Ni}//[\bar{1}10]_{LZO}$ and $[001]_{Ni}//[001]_{LZO}$.

a)Address all correspondence to this author.
e-mail: carmen.jimenez@inpg.fr
DOI: 10.1557/JMR.2009.0162

The pyrochlore structure is more stable against oxygen diffusion due to the more ordered cations structure. $Ln_2Zr_2O_7$ (Ln = lanthanide La to Gd) pyrochlore phases are stable at room temperature (RT) but at high temperature (>1500 °C), an order–disorder transition from pyrochlore to defect fluorite structure occurs. Theoretically, La-pyrochlore does not present such transition.[4] Nevertheless, in thin layers, two phases of LZO have been observed: fluorite and pyrochlore. The presence of the pyrochlore phase can be determined by the (111) and (331) reflections, corresponding to spacing values of 6.24 and 2.48 Å with an intensity of 3% and 5%, respectively, which do not exist in the fluorite structure. The presence of these two reflections in x-ray diffraction (XRD) establishes the presence of pyrochlore structure, but not necessarily in the entire volume: a coexistence of both structures is still possible.[3] The sample has to be probed in thickness to determine the distribution of the crystalline structure. The most adapted technique is high-resolution transmission electron microscopy (HRTEM).

We present a HRTEM study of LZO thin layers grown on $LaAlO_3$ substrates from propinates by MOD and from beta-diketonates by metalorganic chemical vapor deposition (MOCVD). Results obtained in this study can be applied to coated conductors if we consider that the growth mechanisms are independent of substrate. Results on XRD are compared with the electron diffraction obtained by TEM to determine the fluorite or pyrochlore formation. The microstructure of these films is related to the synthesis method and a characteristic feature is the presence of voids in a well-crystallized matrix.

II. EXPERIMENTAL

Lanthanum zirconate was produced by MOD according to a procedure previously described.[5] Lanthanum (III) 2,4-pentadionate and zirconium (IV) 2,4-pentadionate were dissolved in propionic acid (CH_3–CH_2–COOH) to form lanthanum and zirconium propionates. Propionic acid was added to get total cation concentration of 0.6 mol/L. LZO layers were grown on $LaAlO_3$ (LAO) single crystals. LAO presents a rhombohedral structure (Space Group: $R\bar{3}m$, a = 5.364 Å, c = 13.11 Å), but we have preferred to simplify the interpretation by using the pseudocubic (pc) perovskite structure of LAO (Space Group: $Pm\bar{3}m$, 073-3584, a_{pc} = 3.7913 Å). LAO single crystals provided by Crystec GmbH $(00l)_{pc}$ oriented were used as substrates and all diffraction patterns presented in this work are indexed with pseudocubic indices.

Before deposition, the substrates were ultrasonically cleaned in ethanol and acetone during 10 min each. LZO films were deposited by dip coating at RT in a glove box. The substrates were immersed for 30 s in the solution and withdrawn at the rate of 6 cm/min. The samples were dried at 80 °C under infrared lamps for 60 s inside the glove box. The films were then annealed at 960 °C under Ar + 5% H_2 gas flow for 1 h.

YBCO and CeO_2 layers were deposited by pulsed injection (PI) MOCVD on LZO-MOD buffered LAO substrates. A detailed description of the deposition conditions has been presented in Ref. 2. To compare the effect of the deposition method on the LZO microstructure, some LZO layers were also deposited by PI MOCVD on LAO. A single liquid source of $La(tmhd)_3$ and $Zr(tmhd)_4$ precursors dissolved in monoglyme at La/Zr = 1 molar ratio was used for these experiments. The flash evaporation of the solution was performed at 280 °C and the deposition took place at 700 °C under a controlled atmosphere (60% Ar + 40% O_2) at 5 Torr of total pressure.

Film texture and epitaxial relationships among the different layers were determined by XRD in Shultz geometry using a D5000 Siemens four-circle diffractometer with monochromatic Cu K_α radiation (λ = 0.15418 nm). The transport properties of the YBCO layers were evaluated by the determination of J_c (susceptibility measurements).

TEM and electron diffraction were carried out on a JEOL 2011 operating at 200 kV with a 0.19-nm point-to-point resolution. Cross-section samples were obtained by the tripod method. Samples were polished on both sides using diamond impregnated films from 15 μm sequentially down to 0.5 μm until they were less than 15 μm thick. Low-angle ion beam milling was used for final perforation of the samples and to minimize contamination. It is known that the ion milling induces atomic diffusion in the YBCO layer,[6] so observation on the YBCO layer will not be developed in this work. We also observed an YBCO/LZO/Ni structure to confirm the main features on Ni-based substrate. Samples prepared for TEM observation and described in Sec. III have been resumed in Table I.

Energy-filtered transmission electron microscopy (EFTEM) work was performed on a JEOL 3010 microscope operated at 300 kV equipped with a GIF

TABLE I. General description of samples observed by TEM.

Name	Structure on LAO	Deposition method	Film thickness (nm)	I(222)/[I(004) + I(222)] from XRD
LZO1	LZO/YBCO	MOD/MOCVD	80/600	0
LZO2	LZO/CeO_2/YBCO	MOD/MOCVD/MOCVD	80/30/600	0
LZO3	LZO	MOD	80	0.005
LZO4	LZO	MOCVD	400	0.001

post-column energy filter. La, Zr, O, and C mapping were recorded using the La M_{45}, Zr M_{45}, O-K, and C-K edges. The intensity in the map images is proportional to the chemical content. In addition, (t/λ) map was also recorded, which gives information about the thickness of the area with respect to the inelastic mean free.

III. RESULTS

A. LZO obtained by MOD on LAO single crystal

LZO layers (~80 nm thick) were obtained by MOD on LAO single crystals. The annealing conditions were the same for all samples. The name and general description of each sample studied in this work are presented in Table I. As already reported in Ref. 2, XRD analyses of these samples confirm the biaxial texture of the sample. The in-plane texture quantified from φ-scans performed on the (222) reflection is full width half-maximum (FWHM) = 1° and the out-of-plane texture quantified from rocking curves measured on the (004) reflection is FWHM = 0.7°. These results confirm that LZO grains are *c*-axis orientated and that the LZO film nucleates with a biaxial texture over the substrate. The epitaxial relationships of $LaAlO_3$ (as for Ni textured substrate) with LZO are described by $[100]_{LAO}//[110]_{LZO}$ $[010]_{LAO}//[\bar{1}10]_{LZO}$ and $[001]_{LAO}//[001]_{LZO}$.

In the LZO1 sample, YBCO was deposited directly on the LZO buffered LAO substrate. The sample was characterized by third harmonic measurement and a J_c value of 1.15 MA/cm^2 was obtained. In the LZO2 sample, an intermediate buffer layer of CeO_2 was deposited by MOCVD on the LZO layer before YBCO deposition to improve the YBCO performance; the J_c value increased to 2.5 MA/cm^2. The LZO3 sample was not used for YBCO deposition; the LZO layer was characterized by XRD and it showed a sharp texture. The main reflection was the (004), but a small peak corresponding to the (222) reflection was also present in the θ–2θ diffraction diagram. A cross section of an YBCO/LZO/Ni sample was also prepared, which has not been included in Table I. The J_c value on this sample was 0.7 MA/cm^2, and further details have already been presented in Ref. 2. The cross section of this sample allows to determine if there is or not substrate influence.

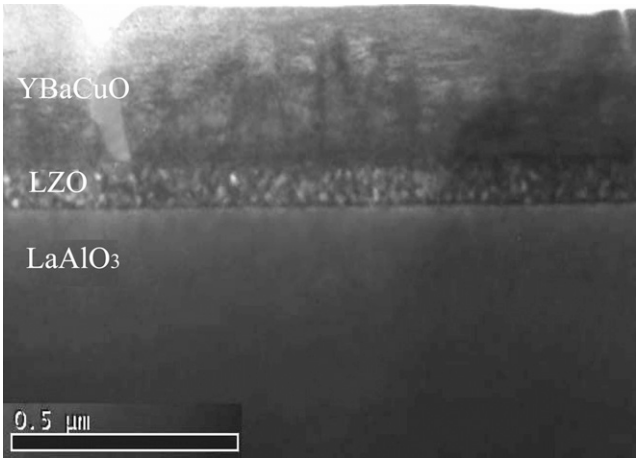

FIG. 1. Bright-field image of the YBCO/LZO/LAO heterostructure corresponding to LZO1 sample.

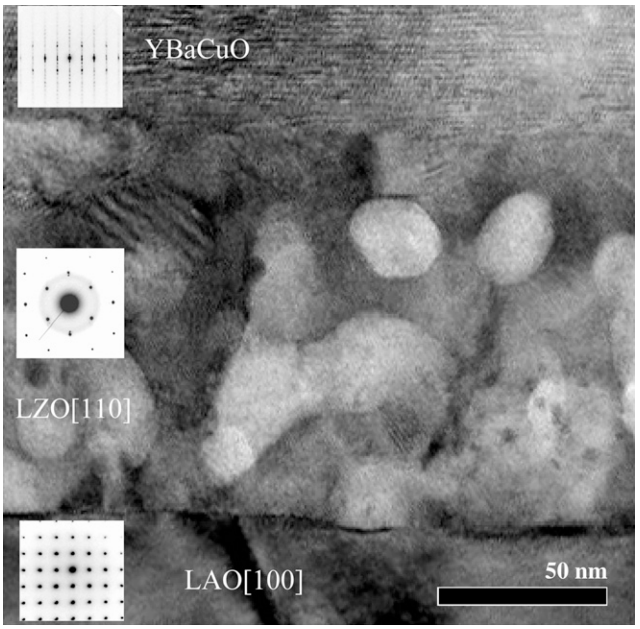

FIG. 2. High magnification image of the LZO layer in the YBCO/LZO/LAO heterostructure corresponding to the LZO1 sample. The LZO layer presents strong variation in contrasts. Diffraction patterns obtained in the LAO [100] pseudocubic (pc) zone axis of the three zones are also presented.

1. Cross section observation

The LZO1 sample was prepared for TEM observation in cross section. A low magnification image of the LZO/LAO heterostructure is presented in Fig. 1. When observed at higher magnification, the LZO layer presents a strong variation in contrast (Fig. 2). The measured thickness, 75 ± 5 nm, corresponds to the expected value. The detected morphology could be interpreted at first sight as polycrystalline grains, but the diffraction patterns obtained in the LAO $[100]_{pc}$ zone axis consist of a single-crystal pattern. Figure 3 presents the electron diffraction pattern of the LAO/LZO interface obtained from a 0.2-μm diaphragm diameter, which has been interpreted as pyrochlore $La_2Zr_2O_7$ ($Fd\bar{3}m$) structure in the [110] LZO zone axis, with the (111) and (311) planes in Bragg diffraction conditions.

The origin of this variation in contrast could be due to three effects: (i) atomic number contrast; (ii) crystallographic contrast; and (iii) density contrast.

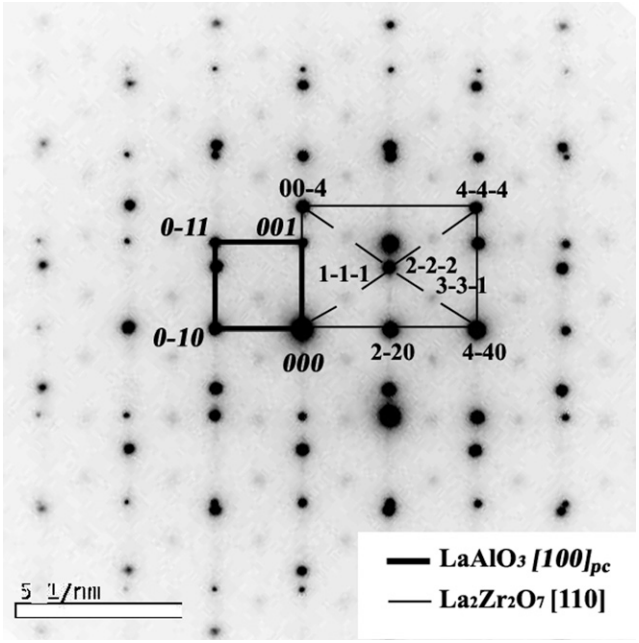

FIG. 3. Diffraction pattern of the LZO/LAO interface from the LZO1 sample obtained in the LAO $[100]_{pc}$ zone axis. The LZO pattern is indexed as pyrochlore as confirmed by the presence of the (111) and (311) reflections. The LAO and LZO unit cells are indicated in the diffraction pattern.

The atomic number contrast would be related to the variation in composition or to the coexistence of several phases. This option is not compatible with the diffraction pattern (Figs. 2 and 3). The crystallographic contrast could explain this variation of contrast if the particles have fluorite structure and the matrix has pyrochlore structure. Images were obtained in bright field [BF, Fig. 4(a)] and dark field [DF, Fig. 4(b)]. All the areas that appear as bright in BF become dark in DF, i.e., all the particles are darker than the matrix in DF. This inversion of contrast indicates that contrast is not due to different structures but to a lower density in the particles than in the matrix. Therefore, the density contrast seems to be the reason for this variation of contrast. Bright zones would correspond to voids placed at different levels of the observed cross section. When changing the focus, Fresnel diffraction fringes appear at the border of these white domains (Fig. 5); this fact corroborates the hypothesis of voids. This explanation has already been presented by Molina et al.[7] in the TEM study of LZO layers. To validate this hypothesis, we tilted the sample to work in another LAO zone axis. When tilting the sample 18.44° around the $[001]_{pc}$ axis, the sample was oriented in the LAO $[3\bar{1}0]_{pc}$ zone axis. The diffraction rules have changed, so crystals oriented in a direction

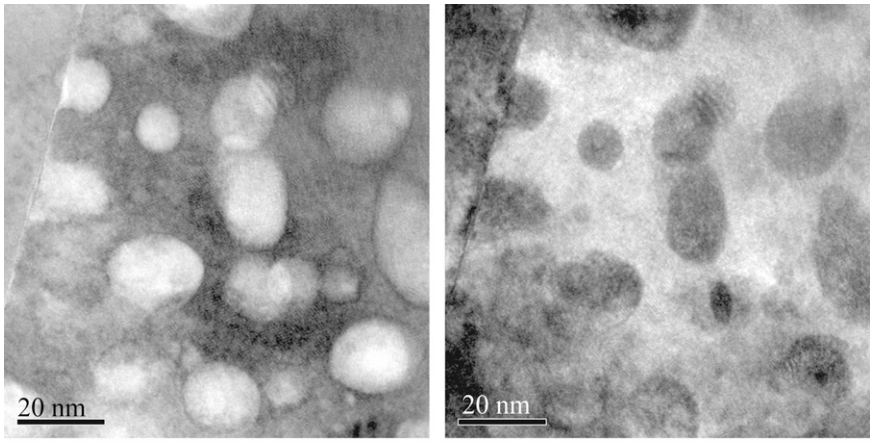

FIG. 4. (a) Bright-field image and (b) dark-field image of the LZO layer.

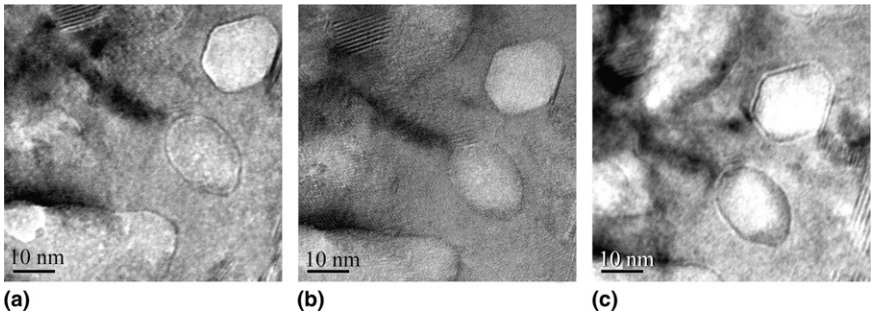

FIG. 5. (b) Focused and (a, c) unfocused TEM images of a cross section of the LZO1 sample. Fresnel fringes in the white zone give evidence of a border.

that does not correspond to this zone axis should disappear. The picture corresponding to the two zone axis is presented in Figs. 6(a)–6(d). No significant differences are visible in these two images; this indicates that contrast does not correspond to crystallographic contrast.

Cross-section observations of the LZO layer were also performed by EFTEM. Figure 7(a) corresponds to the elastic image of the scanned area. We determined the thickness map [Fig. 7(b)], obtained from the t/λ ratio (where t is the thickness of the areas and λ the mean-free path of the electrons in the investigated material, which depends on the incident electron energy and on the collection angle). Energy filtered images (EFTEM) corresponding to energy loss characteristic signal for C, La, Zr, and O were also recorded [Figs. 7(c)–7(f), respectively]. The intensity in the map images is proportional to the chemical content, so these mappings are a qualitative image of the elements distribution.[8] The bright contrast areas on the elastic image appear as a dark area in the La, Zr, and O images. This reduction of intensity in these areas clearly highlights the presence of voids inside the layer. In the (t/λ) map, the dark contrast in the same areas also confirms the presence of voids. On the other hand, C content is low in all the areas and no contrast can be seen between the matrix and the void areas.

Generally, voids or nanovoids seem to be spherical and in other cases, such as in Fig. 8, we could observe hexagonal shapes that would correspond to the (111) plane front. Due to the in-depth distribution of nanovoids, it is difficult to characterize the shape of the voids. The most frequent void size is around 10–20 nm diameter, but it seems that bigger voids are also present. We did not find coalescence of nanovoids in samples observed in this work.

When using high resolution to observe the sample and working in the LAO $[100]_{pc}$ axis zone, there is no discontinuity in the planes, even when crossing zones with different contrast (Fig. 8). Several zones presenting a high variation of contrast at high resolution were scanned, but we did not find grain boundaries, defects, or inclusions in the film. In Fig. 8 we have emphasized the presence of the (111) planes. These planes give evidence of the pyrochlore formation. They are continuous through the particle edge and are visible in almost all the scanned regions. The fast Fourier transform (FFT) of selected areas from this HRTEM are included in Fig. 8; one corresponds to the particle and the other to the matrix. This method was used by Seo et al.[3] to show

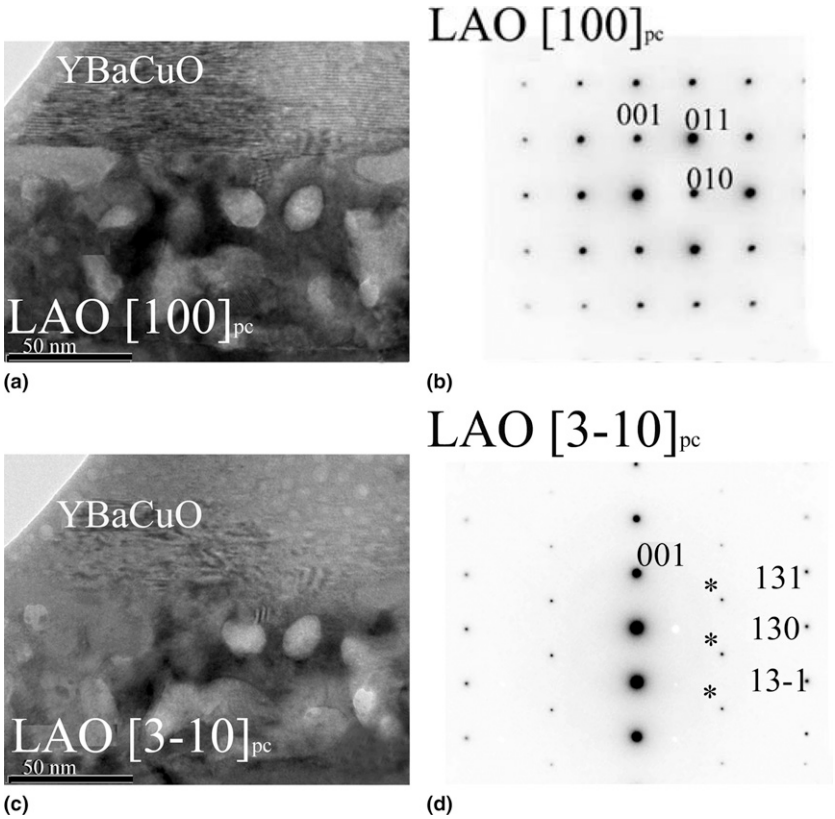

FIG. 6. TEM images of the LZO1 sample in cross section obtained for two zone axis. (a) Image obtained at the YBCO/LZO interface when working in the LAO $[100]_{pc}$ zone axis, (b) LAO diffraction pattern in the LAO $[100]_{pc}$ zone axis, (c) image obtained in the same region as (a) but with a tilt of 18.44° around the [001] axis to work in the LAO $[3\bar{1}0]_{pc}$ zone axis, (d) LAO diffraction pattern in the LAO $[3\bar{1}0]_{pc}$ zone axis. (*indices in this diffraction pattern correspond to the superstructure reflections arising from the rhomboedral structure of LAO).

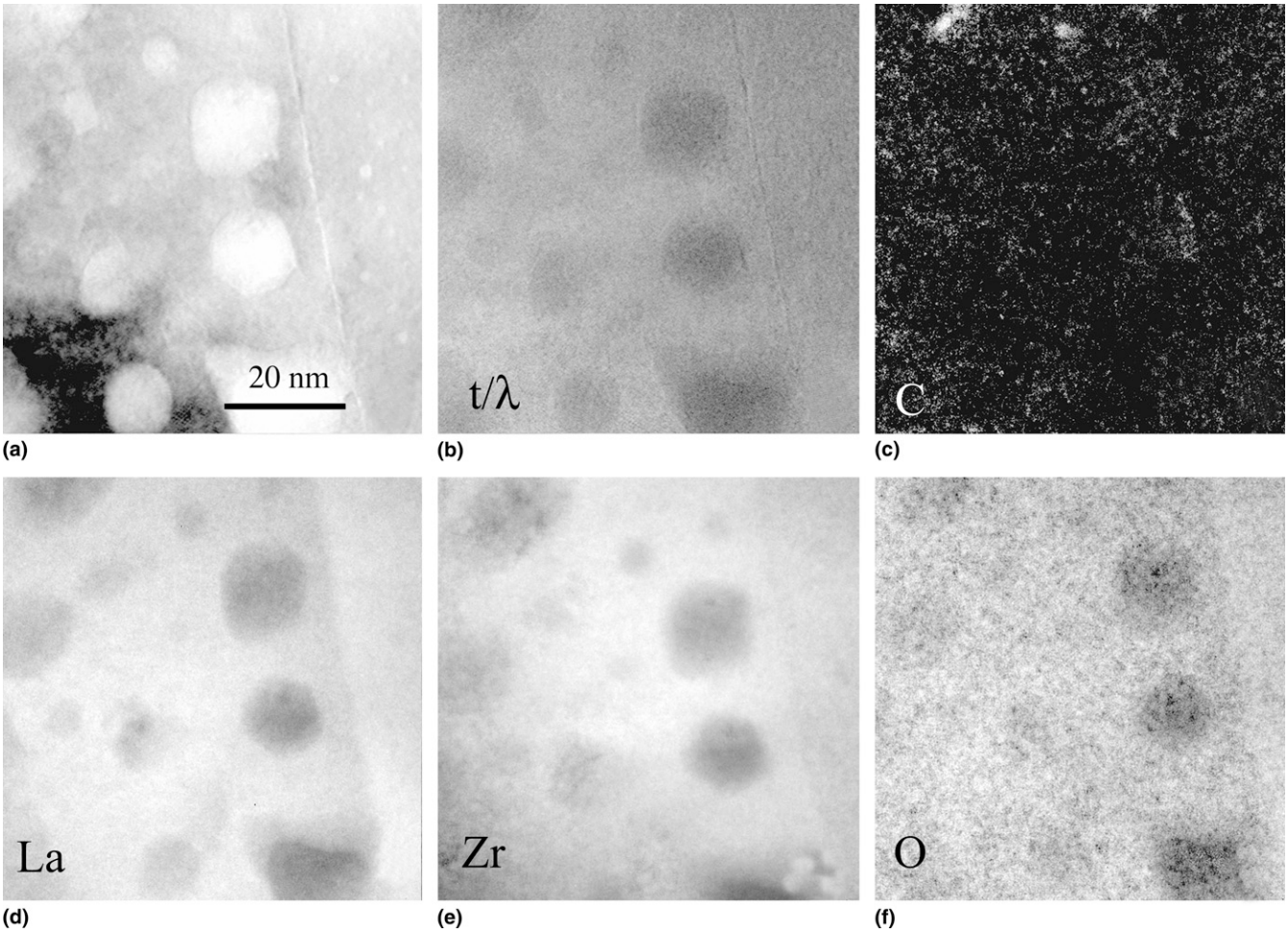

FIG. 7. EFTEM images obtained from a LZO cross section: (a) elastic electron image, (b) thickness map obtained from t/λ, (c) carbon mapping, (d) lanthanum mapping, (e) zirconium mapping, and (f) oxygen mapping.

the simultaneous presence of pyrochlore and fluorite phases. The FFT images confirm the presence of the (111) planes, i.e., the presence of the pyrochlore structure, in all the scanned regions. Moreover, the diffraction patterns obtained with different diaphragm sizes always reflect the pyrochlore structure, without rings or superposed structures (not shown in this work). Taking into account all these results, we can then affirm that fluorite phase does not appear as polycrystalline or textured structure in the LZO1 layer, i.e., that our sample is formed of only single-crystal pyrochlore phase.

When observing the cross section of the LZO2 sample YBCO/CeO_2/LZO/LAO structure, the same features are found as in the LZO1 sample. Despite the irregularities induced by the presence of voids, the interface between the LZO and the CeO_2 layers is well crystallized [Fig. 9(b)] and a very good epitaxial growth characterized by continuous atomic planes is observed. As in the LZO1 sample, LZO crystallizes in pyrochlore phase and the HRTEM pictures of voids show no discontinuity in planes [Fig. 9(c)]. Moreover, the MOCVD CeO_2 layer is very dense and well crystallized [Fig. 9(a)]. The diffraction pattern obtained from the CeO_2/LZO/LAO structure shows a perfect superposition of the fluorite CeO_2 reflections (Space Group: $Fm\bar{3}m$, 34-0394, lattice parameter $a = 5.41134$ Å) on the LZO pyrochlore pattern [Fig. 9(d)]. Nevertheless, the J_c value increases when using CeO_2 as additional buffer layer. This improvement cannot be attributed to a better matching of CeO_2 than LZO with YBCO because their lattice parameters are close. This difference in J_c when depositing directly YBCO on LZO can be explained by the increase of the local interface roughness due to voids.

An YBCO/LZO/Ni sample was also prepared in cross section and the same features as in the previous results were observed in the LZO layer (Fig. 10). The presence of voids was confirmed by defocusing the sample to form the Fresnel fringes and by the continuity of planes in bright and dark contrast regions on HRTEM observations. We will not expose results on these substrates here, investigations are currently being performed and extensive explanation will be given in a future paper.

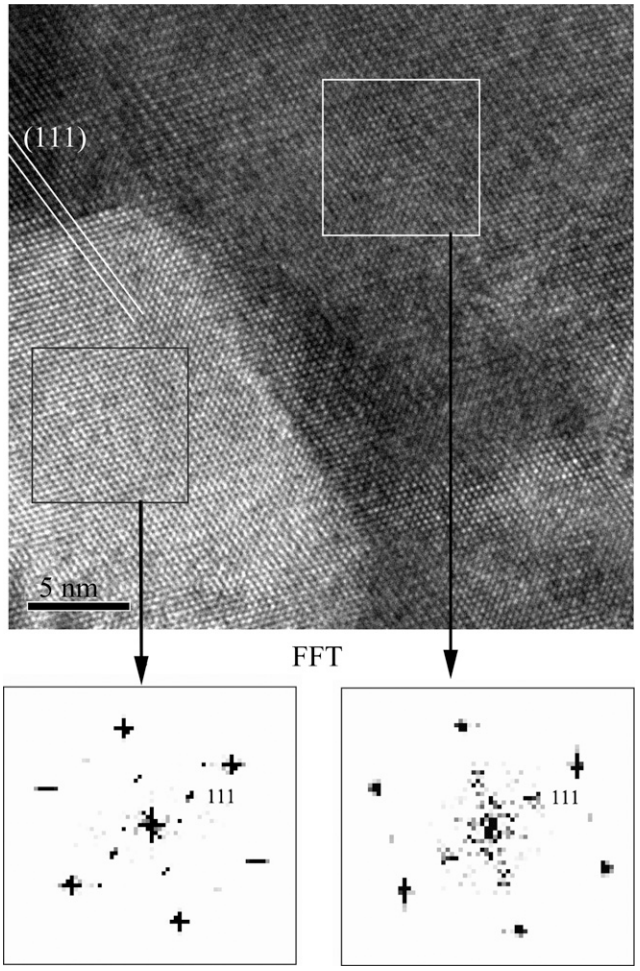

FIG. 8. High-resolution image of the LZO layer showing the contrasted zone formed by a particle and the matrix. The (111) planes crossing the particle edge have been indicated by lines. FFTs of the matrix and the particle show that the (111) planes are present in the entire scanned region.

The LZO3 sample consists of an as-deposited LZO layer, i.e., it was not used as a buffer layer so it was not thermally treated after LZO growth. The crystalline quality of the LZO layer was not tested by the deposition of epitaxial YBCO as in the previous samples, but characterized by XRD. Taking into account the XRD result [Fig. 11(a)], the sample crystalline quality seems to be good enough to be used as buffer layer. Only a small contribution from the (222) reflection can be detected in the logarithmic representation with I(222)/[I(222) + I(400)] = 0.005. The in-plane texture from φ-scans on the (222) reflection was well defined with a FWHM = 1°. Nevertheless, the observations of the cross section by TEM indicate a lower crystalline quality. The layer is divided into two zones, presenting different crystallographic contrast. The layer near the substrate corresponds to the usual pyrochlore LZO phase epitaxially grown on LAO. The layer near the surface is formed by polycrystalline fluorite LZO phase. These results are resumed in the diffraction patterns and in the TEM picture presented in Fig. 11(b). It is important to notice that nanovoids are present in this layer, mainly in the pyrochlore matrix; exceptionally few features, which could be associated to nanovoids, are also present in the polycrystalline fluorite region. The intensity of the (400) reflection was strong (∼1000 cps) and the polycrystalline phase was barely detected by XRD, so it was not possible to deduce from this analysis that the sample was not adapted to transmit the texture to the YBCO layer.

2. Plan view

The LZO1 plan view was prepared by scratching the sample surface to avoid nondesirable effects due to ion milling in the LZO morphology, which could be at the origin of the void formation. The general view of the sample confirmed the presence of voids [Fig. 12(a)], which are homogeneously distributed in the sample surface. The diffraction pattern obtained in the LAO $[001]_{pc}$ zone axis showed a cubic structure that can be equally attributed to fluorite or to pyrochlore, because in this zone axis there is not structural difference [Fig. 12(c)]. We indexed it as pyrochlore structure according to the cross-section observation of the same sample. The HRTEM pictures showed the continuity of atomic planes across contrasted zones [Fig. 12(b)].

B. LZO obtained by MOCVD on LAO single crystal

LZO layers obtained by MOCVD were compared to those obtained by MOD to determine if voids are intrinsic to LZO or related to the synthesis process (LZO4). The MOCVD sample was not used for YBCO deposition. The XRD analysis of this sample showed a sharp texture [Fig. 13(a)]. The main reflection was the (004), but a small peak corresponding to the (222) reflection was also present in the θ–2θ diffraction diagram, i.e., I(222)/[I(222) + I(400)] = 0.001. The sample was observed by TEM in cross section. A general view of the cross section showed a columnar structure of a 400-nm-thick film [Fig. 13(b)]. The structure is compact near the interface and through the thickness to around 300 nm, and then a columnar morphology appears on the external 50 nm; columns are completely separated at the surface. A view of the interface showed a good epitaxy [Fig. 13(c)] as in the MOD LZO layer and some dislocations probably due to strain relaxation. The diffraction pattern confirmed the crystallization in pyrochlore structure [Fig. 13(d)]. Three samples obtained by MOCVD were observed by TEM and the absence of voids was confirmed in all of them. We can infer that voids observed in the LZO layers obtained by MOD are due to the synthesis process, and therefore to the pyrolysis reaction taking place during the annealing.

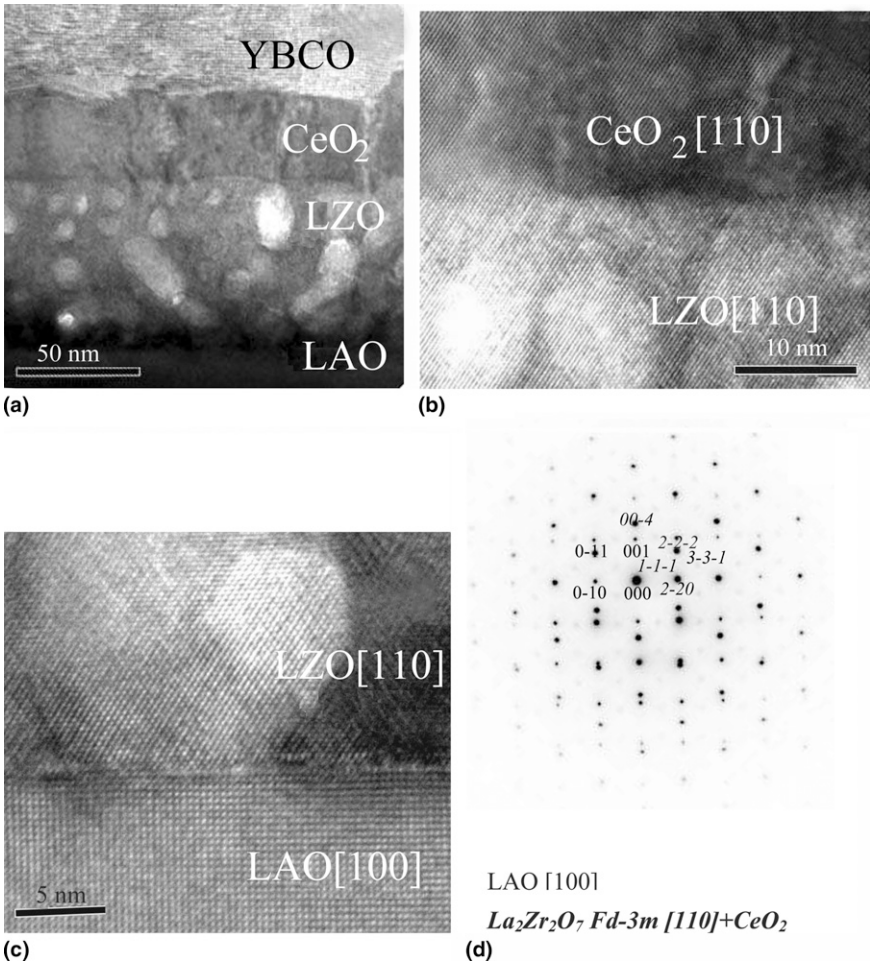

FIG. 9. TEM images of the YBCO/CeO_2/LZO/LAO heterostructure cross section from the LZO2 sample. (a) Low-resolution images of the LZO/CeO_2/YBCO heterostructure. The CeO_2 layer is very compact without voids. (b) High-resolution image of the CeO_2/LZO interface showing the excellent epitaxy of the CeO_2 layer. (c) High-resolution image of the LZO/LAO interface showing the excellent epitaxy of the LZO layer. (d) Diffraction pattern of the structure. The CeO_2 pattern overlaps with the LZO pattern and no additional reflections are detected. This diffraction confirms the presence of the (111) and the (311) planes corresponding to pyrochlore phase.

IV. DISCUSSION

Results presented in this work agree with other publications of TEM images made by other groups, even if we used $LaAlO_3$ as substrate instead of nickel. These groups have shown the same morphology on samples grown on Ni RABiTS by an equivalent MOD process.[7,9–12] As described earlier (Fig. 10), some TEM observations on an YBCO/LZO/Ni sample were performed, and the presence of voids was also confirmed. We can then consider that growth mechanisms in MOD are independent of substrate. We will focus in this section on the similarities and on the differences found in TEM observations as compared with previous works.

Current investigations on LZO grown by MOD are based on two kinds of metalorganic precursors. Paranthaman et al.[10] have obtained good results starting from a solution of La isopropoxide and zirconium n-propoxide in n-propanol and 2-methoxy ethanol, which presents the significant disadvantage to be teratogen. The cross section of a multilayer sample showed the same voids, but the authors did not comment on this morphological aspect. An HRTEM image is presented in Ref. 11 with a sharp and well-crystallized LZO/Ni interface. There are no voids in the observed region, but they do not show a general view of the layer. In another paper, Heatherly et al.[12] showed a TEM picture of the cross section of a LZO layer on Ni–W substrate with the same characteristic contrast, mainly concentrated at the interface. Near the surface a mixture of a dense material and regular shapes is detected. The authors did not identify them as voids, but they claimed that the films are composed of a LZO pyrochlore matrix and of LZO fluorite particles.

On the other hand, a group in Dresden is working with another chemical approach similar to our chemical MOD route: lanthanum (III) 2,4-pentadionate (with a 2.77 H_2O calculated) and zirconium (IV) 2,4-pentadionate

as educts, and acid propionic (CH_3–CH_2–COOH) as solvent. An interesting paper was published by this group,[7] which gives evidence of the presence of voids. Tilt measurements are equivalent to our results.

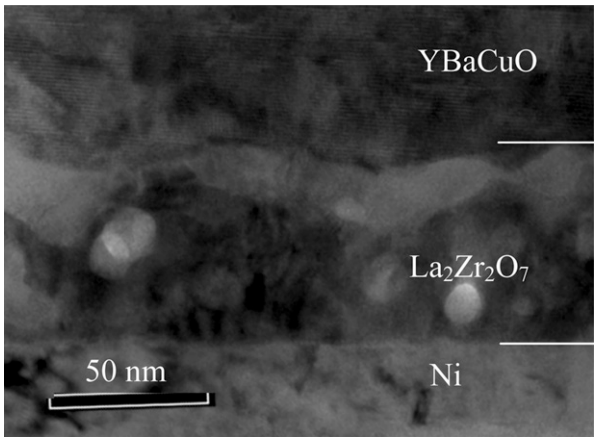

FIG. 10. TEM image of the YBCO/LZO/Ni heterostructure in cross section showing the characteristics voids in the LZO layer.

They found grains with a diameter from 100 to 300 nm depending on annealing temperature. Grain formation could be related to nickel structure, although they are smaller than nickel grain (40 μm). They interpreted the crystal structure as pyrochlore, even if there was no visible evidence of (111) planes in the diffraction pattern.[9] In some cases, diffraction rings appear showing a local poor texture, which could not be detected by XRD. They established nanovoids as a typical feature for MOD-grown LZO buffer layers. Nevertheless, they did not show any HRTEM observation of the sample in this work.

In our study, crystalline quality seems to be better than in precedent works: rings are not visible in any diffraction pattern and LZO grain boundaries are not detected. HRTEM observations showed the continuity of the crystallographic planes at nanometric scale, and diffraction patterns confirmed the texture on submicron scale. This high crystalline quality can be due to the use of a single-crystal substrate, and it is also reflected in the in-plane and out-of-plane FWHM values as compared to

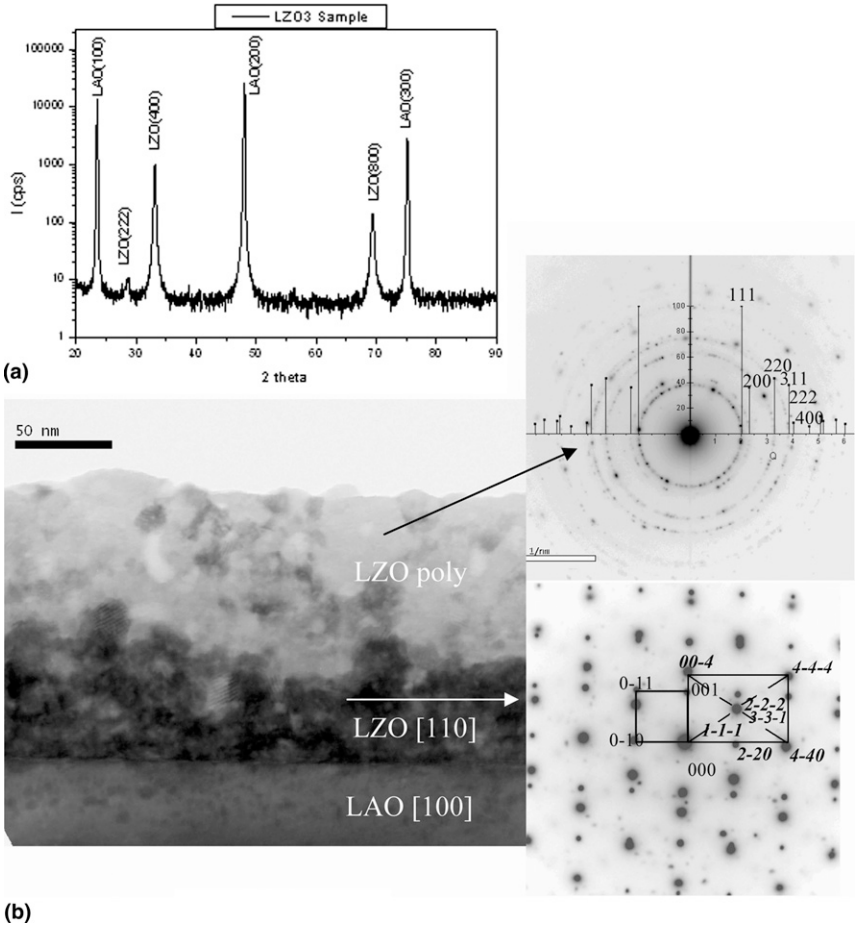

FIG. 11. Characterization of the LZO3 sample (a) XRD diagram in θ–2θ configuration. (b) TEM image on cross section showing two crystallographic contrasts. Diffraction pattern of each zone are included: pyrochlore epitaxial phase at the LAO interface and polycrystalline fluorite phase at the surface.

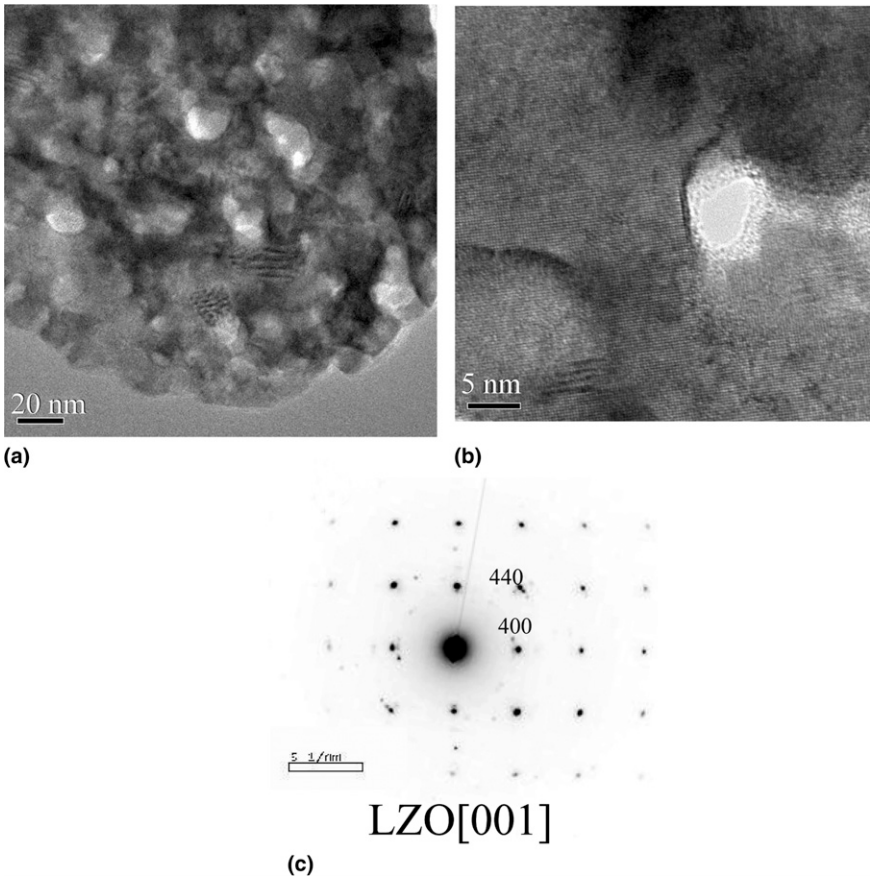

FIG. 12. Plan view of the LZO1 sample. (a) A general view of the layer showing the voids presence in the film. (b) High-resolution images of the LZO1 sample in plan view showing a good continuity of planes through the layer. This region is thin and the beam directly crosses through the void. (c) Diffraction pattern of the observed region, corresponding to the LZO [001] zone axis.

LZO on RABiTs.[2] We should confirm this hypothesis about grain formation in further TEM observations of Ni-based samples. Nevertheless, we can already affirm that the formation of nanovoids is not substrate dependent (Ni or LAO), or a LZO intrinsic feature (voids are not present in pyrochlore MOCVD layers).

The mechanisms involved in the MOD process are the only explanation for the apparition of these cavities, probably corresponding to two involved steps: pyrolysis and crystallization. The decomposition of the metal-organics precursors occurs during the annealing in Ar + H_2 atmosphere. Our thermal profile consists in a heating ramp at 450 °C/h up to 950 °C, and the temperature is then maintained at 950 °C for 30 min. The cooling rate is not controlled. Pyrolysis takes place during the first part of the annealing at low temperature (RT-500 °C), and crystallization occurs at higher temperatures. As analyzed by Bhuiyan et al.,[13] the crystallization driving force determines the probability to obtain bulk nucleation or interface nucleation. The crystallization driving force depends on the free energy of the two material states and on the temperature at which crystallization occurs. A smaller driving force enhances the interface nucleation. A way to decrease the crystallization driving forces is to use high heating rates, which would delay the densification and crystallization processes to higher temperatures. To get LZO textured samples (in principle in the pyrochlore structure because it is the more stable phase), heterogeneous nucleation should start at the substrate interface: the texture template can only be obtained from substrates. The crystallization front starts at the interface and should expand on the film thickness toward the surface. If homogeneous nucleation appears somewhere in the film, a nontextured phase will crystallize, because there is no preferential direction for crystallization as observed in LZO3 sample. A heterogeneous nucleation mechanism permits to explain a better crystalline quality of LZO on LAO than on nickel: nontextured nucleation sites on Ni (i.e., grain boundaries in Ni) are more probable during heterogeneous nucleation, so texture template has a higher quality in LAO than in Ni. Moreover, it can also explain the formation of voids. The epitaxial crystallization front should move fast to be more favorable than homogeneous nucleation. As the crystallization front expands, the porous morphology created during pyrolysis by the relaxed products

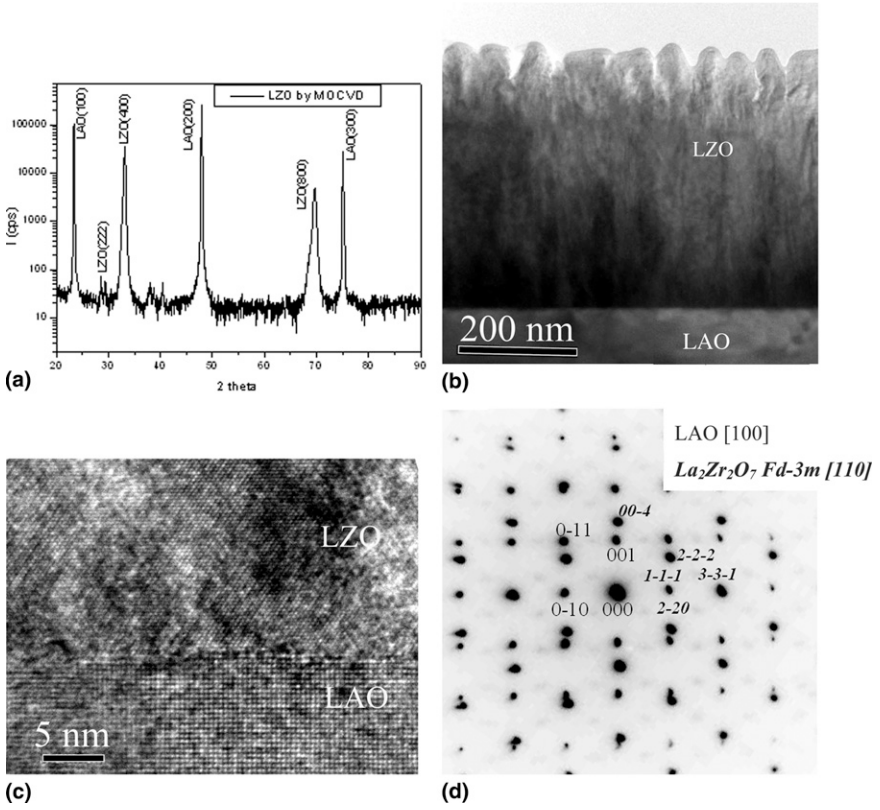

FIG. 13. Characterization of the LZO4 sample consisting of a LZO layer deposited by MOCVD on LAO. (a) XRD diagram in θ–2θ configuration. (b) General view of the structure in cross section in the LAO $[001]_{pc}$ zone axis. No voids are visible in the LZO layer. (c) High-resolution image of the LZO/LAO interface. A sharp and well-defined interface is visible. (d) Diffraction pattern in the LAO $[001]_{pc}$ zone axis of the observed region. The structure is interpreted as pyrochlore structure due to the (111) and (311) planes presence.

is crystallized. An unanswered question is, "Are the voids empty or filled with these products?" The EFTEM analysis shows that carbon content is almost zero and that the concentration is homogenous in the two contrasted zones. We can then infer that there are no residues in the voids, and that the pyrolysis was completed before nucleation started.

It has been observed in the $YBCO_{MOD}/CeO_{2RF}/LZO_{MOD}/Y_2O_{3PVD}$/Ni structure[10] that polycrystalline NiO and $NiWO_4$ phases are formed at the Y_2O_3/Ni interface, which means oxygen diffuses through the LZO layer. This result is not compatible with the diffusion barrier properties of LZO.[14] The voids in LZO can be at the origin of the oxygen diffusion through the layer. The effective thickness is smaller and films have to be thicker to reduce oxygen diffusion. This point is important in the optimization of the architecture of coated conductors.

Despite the presence of voids, the J_c values obtained from our LZO structures are really encouraging (1.5 MA/cm^2 for the $YBCO_{MOCVD}/LZO_{MOD}$/LAO structure and 2.5 MA/cm^2 for the $YBCO_{MOCVD}/CeO_{2MOCVD}/LZO_{MOD}$/LAO structure[2]). The voids do not seem to be a limiting factor for using LZO obtained by MOD as buffer layer in coated conductors.

V. CONCLUSIONS

LZO layers obtained by chemical methods (MOD and MOCVD) were characterized by TEM and HRTEM. The study focused on the local crystal structure determined by electron diffraction and by high-resolution images to identify the local distribution of the pyrochlore and fluorite phases. A characteristic feature of LZO thin film deposited by MOD is the formation of voids in an almost single-crystal structure of LZO pyrochlore phase. The most frequent void size is 10–20 nm for our annealing conditions. For comparison, LZO layers deposited by MOCVD were also studied. In this last case, the film is compact without voids and the structure corresponds to the pyrochlore phase. The formation of voids takes place when depositing the LZO layer on LAO and on nickel substrates, so it is not substrate dependent. We conclude that voids are a characteristic feature of MOD grown films and are related to the pyrolysis and growth mechanisms. Considering the J_c values obtained from LZO structures, voids do not seem to be a limiting factor for using LZO obtained by MOD as buffer layer in coated conductors, but they should be taken into account for the optimization of the architecture of coated conductors.

ACKNOWLEDGMENTS

This work has been financially supported by the French Research National Agency (ANR) through the Matériaux et Dispositifs Supraconducteurs pour l'Energie (MADISUP) Project and by Région Rhône-Alpes Système Électrique Supraconducteur à courant continu (SESUC) project. We acknowledge Dr. Ph. Odier (Institut Louis Néel—CRETA) for the fruitful discussions and Dr. A. Abrutis (Vilnius University) for the collaboration in the MOCVD process.

REFERENCES

1. Y. Shiohara, M. Yoshizumi, T. Izumi, and Y. Yamada: Present status and future prospect of coated conductor development and its application in Japan. *Supercond. Sci. Technol.* **21,** 034002 (2008).
2. T. Caroff, S. Morlens, A. Abrutis, M. Decroux, P. Chaudouët, L. Porcar, Z. Saltyte, C. Jiménez, P. Odier, and F. Weiss: $La_2Zr_2O_7$ single buffer layer for YBCO RABiTs coated conductors. *Supercond. Sci. Technol.* **21,** 075007 (2008).
3. J.W. Seo, J. Fompeyrine, A. Guiller, G. Norga, C. Marchiori, H. Siegwart, and J.P. Locquet: Interface formation and defect structures in epitaxial $La_2Zr_2O_7$ thin films on (111) Si. *Appl. Phys. Lett.* **83**(25), 5211 (2003).
4. M.A. Subramanian, G. Aravamudan, and G.V. Subba Rao: Oxide pyrochlores—A review. *Prog. Solid State Chem.* **15,** 55 (1983).
5. Z.M. Yu, P. Odier, L. Ortega, L. Zhou, P.X. Zhang, and A. Girard: $La_2Zr_2O_7$ films on Cu–Ni alloy by chemical solution deposition process. *Mater. Sci. Eng., B* **130,** 126 (2006).
6. J. Ayache and P.H. Albarede: Application of the ionless tripod polisher to the preparation of YBCO superconducting multilayer and bulk ceramics thin films. *Ultramicroscopy* **60,** 195 (1995).
7. L. Molina, K. Knoth, S. Engel, B. Holzapfel, and O. Eibl: Chemically deposited $La_2Zr_2O_7$ buffer layers for YBCO-coated conductors: Film growth and microstructure. *Supercond. Sci. Technol.* **19,** 1200 (2006).
8. P. Bayle-Guillemaud, A. Barbier, and C. Mocuta: Development of a quantitative energy filtering TEM method to study a reactive NiO/80Ni20Fe interface. *Ultramicroscopy* **88,** 99 (2001).
9. K. Knoth, R. Hühne, S. Oswald, L. Molina, O. Eibl, L. Schultz, and B. Holzapfel: Growth of thick chemical solution derived pyrochlore $La_2Zr_2O_7$ buffer layers for $YBa_2Cu_3O_{7-x}$ coated conductors. *Thin Solid Films* **516,** 2099 (2008).
10. P. Paranthaman, S. Sathyamurthy, M.S. Bhuiyan, P.M. Martin, T. Aytug, K. Kim, M. Fayek, K.L. Leonard, J. Li, A. Goyal, T. Kodenkandath, X. Li, W. Zhang, and M.W. Rupich: MOD buffer/YBO approach to fabricate low-cost second generation HTS wires. *IEEE Trans. Appl. Supercond.* **17**(2), 3332 (2007).
11. S. Sathyamurthy, M. Paranthaman, H.Y. Zhai, T. Ayung, C. Cantoni, K.J. Leonard, E.A. Payzant, H.M. Christen, A. Goyal, X. Li, U. Schoop, T. Kodenkandath, and M.W. Rupich: Chemical solution deposition of lanthanum zirconate barrier layer applied to low-cost coated conductor fabrication. *J. Mater. Res.* **19**(7), 2117 (2004).
12. L. Heatherly, H. Hsu, S.H. Wee, J. Li, S. Sathyamurthy, M. Paranthaman, and A. Goyal: Slot die coating and conversion of LZO on rolling assisted biaxially textured Ni–W substrates with and without a very thin seed layer in low vacuum. *IEEE Trans. Appl. Supercond.* **17**(2), 3417 (2007).
13. M.S. Bhuiyan, M. Parnathamn, and K. Salama: Solution-derived textured oxide thin films—A review. *Supercond. Sci. Technol.* **19,** R1 (2006).
14. X.Q. Cao, R. Vassen, W.S. Jungen, S. Schwartz, F. Tietz, and D. Stöver: Thermal stability of lanthanum zirconate plasma sprayed coating. *J. Am. Ceram. Soc.* **84**(9), 2086 (2001).